

August 1964

G3/14

CORNELL UNIVERSITY  
CENTER FOR RADIOPHYSICS AND SPACE RESEARCH  
Ithaca, N. Y. 14850

June 1970

CRSR 451

A SEARCH FOR LIFE ON EARTH AT  
100 METER RESOLUTION

Carl Sagan and David Wallace

Laboratory for Planetary Studies

Cornell University

Ithaca, N. Y. 14850

### Abstract

A study of several thousand photos indicates that  $\sim 10^{-2}$  Gemini and Apollo photographs of the Earth at 100 m resolution reveal signs of life -- rectangular arrays due to human agricultural and urban territoriality, roads, canals, jet contrails, and industrial pollution. Potential false positives -- e.g., dunes, sand bars, jet stream clouds -- abound. A curve is derived for the detectivity of contemporary life on Earth, in a plot of ground resolution versus global coverage. A comparable biology on Mars would not have been detected by all observations of Mars through Mariner 7. Forthcoming Mars orbiter and lander imaging experiments hold significant promise of detecting life on Mars of contemporary terrestrial extent and advancement, should such life exist.

Because the close-up reconnaissance of another terrestrial planet, Mars, is imminent, it is of some interest to reconsider the appearance of our own planet as seen from space. Some years ago a study was published (Kilston, Drummond and Sagan, 1966) which analyzed several thousand Tiros and Nimbus photographs of the Earth taken at  $\sim 1$  km resolution. It was found that, particularly for the manifestations of biology on the planet Earth, such photographs were generally uninteresting. No sign of major engineering works or of the largest metropolises could be found. It was argued that, for reasons of economy and geometry, technical civilizations tend to construct rectilinear features which have a markedly artificial appearance. But the number of such rectilinear features visible at 1 km resolution are very few. It was concluded that 1 in  $\sim 10^3$  Tiros and Nimbus photos of the Earth showed signs indicative of our technical civilization; and that a significant number of false positives existed even in that data set -- e.g., natural peninsulas, self dunes, sand bars, and possibly jet stream clouds. Had the Mariner 4 space vehicle been directed at the Earth rather than at Mars and roughly 20 photographs of no better than 1 km resolution acquired, no sign of life, intelligent or otherwise, would have been discerned on Earth.

Since that time approximately one order of magnitude more photographs of Mars have been obtained by Mariners 6 and 7; and, as of this writing, one to two orders of magnitude further improvement can be expected by United States and Soviet Mars orbiters in 1971-72. In these missions resolutions  $\sim 100$  meters

are obtainable. Accordingly it is of interest to continue our calibration studies and examine the Earth at  $\sim 100$  m resolution. Fortunately the successful series of Gemini and Apollo manned missions has produced a very rich library of high resolution color photographs of the Earth. With the cooperation of the Goddard Space Flight Center and particularly of Dr. Paul D. Lowman, Jr., we have examined several thousand Gemini and Apollo photographs in an attempt to detect life on Earth. Photographs from Gemini 3-12 and Apollo 6 and 9 were inspected. Displayed in Table I are the relevant particulars of camera and film for those photographs selected in this study. Ordinary color film was used in all magazines relevant here, except for Magazine 26 of Gemini 7, where infrared Ektacrome, a camouflage detection film, was employed. Focal lengths ranged from 38 mm on Gemini 9 and 11 to a 250 mm telephoto lens on Gemini 7. Slant ranges varied from 160 km on Gemini IV to 1200 km on Gemini XI. Photographs were taken with viewing angles (the angle between the line of sight and the local planetary normal) ranging from  $0^\circ$  to  $90^\circ$ .

For a typical photograph, taken with 80 mm focal length at  $f/11$ , the Rayleigh criterion for yellow light gives a diffraction limit of  $8.4 \times 10^{-5}$  radians, corresponding at 200 km altitude to a ground resolution of 17 m. With a  $1/250$  sec exposure time, the 8 km/sec orbital velocity implies a resolution limit due to motion smearing of 32m. Spacecraft jitter and hand motion will degrade this figure still further. If

there are  $10^4$  resolution elements due to grain across the 70 mm negative, the Gaussian lens equation yields, for the same altitude and focal length as before, a grain-limit to the ground resolution of 35 m, where we have assumed a resolution criterion of two grains. Less fine-grain film yields proportionately inferior ground resolutions. The three effects taken together make it very unlikely that, even in the best cases (e.g., Gemini VII-22-3, Fig. 20, or IV-8-3), the effective ground resolution was better than 50 m; typical values for the images of the present study are  $\sim 100$  m (cf. Table II).

Figures 1 through 28 exhibit some of the more interesting results. Figures 1 through 7 are reproduced here in color.\* Figures 8 through 28 are displayed in black and white, although they were originally taken in color. After these photographs were originally examined and selected at GSFC, color reproductions were obtained from the Technology Application Center, University of New Mexico, Albuquerque, New Mexico for further study at Cornell. The photographs shown here were prepared by Mr. Herman Eckelmann of Cornell's Center for Radiophysics and Space Research from the New Mexico color transparencies. Some loss of definition in the successive printings is inevitable, particularly in the conversion from color to black and white, but at least many of the features of interest can still be discerned in the reproductions shown here.

Approximately 1800 photographs were inspected with some care. These were largely, if not exclusively, in cloudfree

\*[In black-and-white in this preprint.]

areas. Since the Earth is on the average 50 percent cloud covered, this corresponds to an effective non-selective inspection of 3600 photographs of the same resolution. Some selection effect is apparent in the original statistics: the astronauts were not photographing the Earth entirely at random, but rather were photographing regions which had particular associations for them or which appeared to be visually of interest. Consequently technological artifacts were to some degree weighted preferentially. We attempt to partially normalize for this selection effect by neglecting duplicate pictures taken of the same area. Of these 3600 (effective) photographs, 106 were selected as deserving further study. These photos are described in Table II. Of these, 60 of the features of interest have been classified as geological and 20 as meteorological in origin. Some phenomena such as dunes (cf. Figs. 17, 19 and 20) are undeniably rectilinear, but are not of biological origin. On the other hand, other phenomena such as coral atolls (cf. Fig. 25) are undeniably of biological origin, but would almost certainly not be so identified on the basis of their geometry without further knowledge of terrestrial biology. Some river basins have remarkably striking geometry as seen from space (Figs. 14-16) as do some cloud features (Figs. 1, 8, and 9). Likewise sandbars (Figs. 2, 18 and 24) and craters (Figs. 22 and 23) have striking geometries but are not indicative of life on Earth.

But a sizeable number (57) of the selected photos (cf. Figs. 3-7, 26-28) are so regularly geometrized as to defy

nonbiological explanations. These pictures break down as follows: roads, 29; canals, 5; agricultural geometrizing of the environment, 15; jet contrails, 4; industrial pollution, particularly smoke stack plumes, 4. Some photographs have been classified in more than one category. Some cities laced with extensive roads (e.g., Dallas-Fort Worth, Fig. 5) are easily detectable; other cities of large size (e.g., Cairo, Fig. 7) are much less detectable. Perhaps the most striking signs of intelligent life on Earth are the checkerboard patterns of agricultural and urban territoriality (e.g., Figs. 3-6). Nature paints with a broad brush, but Man, with a culture far from global, is a pointillist.

The fraction of photographs of roughly 100 m resolution which show signs of intelligent life is then  $57/3600 \approx 1.5\%$ . Allowing for astronaut selection effects, we end up with 1% as the effective value for the fraction of photographs showing signs of life.

These results can now be used in a more general study of the photographic detectivity of hypothetical biology on a given planet. We have found that  $\sim 1\%$  of Apollo and Gemini photographs of the Earth at  $\sim 0.1$  km resolution are indicative of life. Kilston, Drummond and Sagan (1966) found that  $\sim 0.1\%$  of 1 Km resolution. Tiros and Nimbus photographs of the Earth are indicative of life. With improved resolution it is clear that the detectivity increases rapidly and that, with a resolution of several meters, especially at low sun, it is possible that only a few

randomly placed photographs over the surface area of the Earth would be adequate to detect life at the present state of terrestrial biology and technology (see, e.g., Sagan et al. 1966; Sagan, 1970). On the other hand at resolutions considerably poorer than 1 km it is apparent that even complete photographic coverage of the Earth would be unsuccessful in detecting life. These detection thresholds have been translated into the rippled curve in Figure 29 marked "Detectivity Threshold, Contemporary Life on Earth," where the surface resolution is plotted against the fraction of the disc ( $4\pi R^2$ ) observed. The latter quantity is obtained from the photographs in question through the appropriate number of resolution elements per picture and the assumption that two resolution elements are required for a physically significant resolution of detail. Also shown in the same figure are a hypothetical detectivity threshold for a planet like the Earth in the absence of intelligent life -- as, for example, the Earth some millions of years ago; and a hypothetical detectivity threshold for a planet with a technical civilization somewhat in advance of our own -- where it is assumed that a rather largescale geometric reworking of the planetary surface has occurred.

While there is no a priori reason to believe that Mars is or was inhabited by life, intelligent or otherwise, it is instructive to plot on the same diagram the actual observations of Mars which have been performed to date, and which are anticipated in the next few years. In Figure 29 is displayed

a curve of the sum total of human observations of Mars through the 1969 Mariner Mars missions, adopted from a calculation of Murray et al. (1971). In the same figure we have anticipated the corresponding curve for Mariner 9 and Mars 2 and 3 (cf. Masursky, et al., 1970). At the time of writing the actual mission strategies of these space vehicles remains somewhat uncertain and is the cause of the large error indicated. Finally Figure 27 also shows a single point corresponding to the poorest resolution (towards the local horizon) of the currently anticipated Viking Lander Imaging Systems (cf. Mutch et al., 1971), assumed randomly emplaced on Mars; i.e., independent of any forthcoming information about biologically promising landing sites.

We find that the observations through Mariner 6 and 7 would not have detected even the hypothetical advanced technical civilization on Mars -- much less contemporary terrestrial life. This finding underscores the futility of arguing, from the absence of recognizable signs of life in the Mariner 4, 6 or 7 photographs, that Mars is uninhabited. On the other hand, we see that the Mars 1971 Orbiters will be able to detect an advanced technical civilization of the sort hypothesized in Figure 29, and have at least a modest chance of detecting a level of civilization on Mars comparable to the contemporary terrestrial civilization. The anticipated Viking Mars Orbiters represent an additional small improvement (cf. Carr et al. 1971). Significantly, the Viking Lander cameras have a rather good chance of detecting contemporary

life on Earth, even in the absence of our technical civilization -- particularly if some wisdom is used in landing site selection. Thus we conclude that were life on Mars at the same level of detectivity as contemporary life on Earth, it would have a significant prospect of being detected in the next few years. More primitive life would of course elude detection longer.

Acknowledgement:

This research was supported in part by NASA/JPL Contract 952487 and in part by NASA Grant NGR 33-010-101. We are particularly grateful to Dr. Paul G. Lowman, Jr. of the Goddard Spaceflight Center for helping us gain access to the Gemini and Apollo photographs, and for several helpful suggestions.

TABLE I

FLIGHT	CAMERA	LENS	FILM
Gemini IV	Hasselblad 500c	Zeiss Planar 80mm f/2.8	Ektachrome S.O. 217
Gemini V Magazines 1-3	Hasselblad 500c	Zeiss Planar 80mm f/2.8	Ektachrome S.O. 217
Gemini V Magazine 4	Hasselblad 500c	Zeiss Planar 80mm f/2.8	Ansochrome D-50
Gemini VI	Hasselblad 500c	Zeiss Planar 80mm f/2.8	Ektachrome S.O. 217
Gemini VII Magazines 13, 17, 22, 24	Hasselblad 500c	Zeiss Planar 250mm f/4.5	Ektachrome S.O. 217
Gemini VII Magazine 26	Hasselblad 500c	Zeiss Planar 80mm f/2.8	IR Ektachrome 8443
Gemini IX Magazines B,C	Hasselblad 500c	Zeiss Planar 80mm f/2.8	Ektachrome S.O. 217
Gemini IX Magazine D	Hasselblad Super Wide Angle	Zeiss Biogon 38mm f/4.5	Ektachrome S.O. 217
Gemini IX Magazine F	Not stated	Not stated	Ektachrome S.O. 217
Gemini X	JA Mariner 70 mm Space Camera	Xenotan 80mm f/2.8	Ektachrome S.O. 217
Gemini XI Magazine 8	Hasselblad Super Wide Angle	Zeiss Biogon 38mm f/4.5	Ektachrome MS S.O. 3.68
Gemini XI Magazine 11	JA Mariner 70mm Space Camera	Xenotan 80 mm f/2.8	Ektachrome MS S.O. 368

Table I, cont.

FLIGHT	CAMERA	LENS	FILM
Gemini XII	Hasselblad Super Super Wide Angle	Zeiss Biogon 30mm f/4.5	Ektachrome MS S.O.368
Apollo 6	Mariner, Model 220G	Kodak Ektar 76mm f/2.8	Ektachrome High Resolution Aerial S.O.121
Apollo 9	Hasselblad 500c	Zeiss Planar 80mm f/2.8	Ektachrome S.O.368

Table II  
Summary of 106 Selected Gemini and Apollo Images

<u>Mission</u>	<u>Mag</u>	<u>Frame</u>	<u>Location</u>	<u>Items of Interest</u>	<u>Contrast</u>	<u>Altitude (Miles)</u>	<u>Angle of Photograph</u>	<u>Slant Range</u>	<u>Resolution</u>	<u>Focal Length</u>
Gemini IV	6	9	Hunan Province China	Hsiang River contains straight sections forming angles	med	(100-175)	Vertical	175 mi	0.2 Km	80 mm
	8	3	Baja California Mouth of Colorado River	Sinuuous tidal drain- age channel. See also AS6-2-1435	med	102	Vertical	102 mi	0.1 Km	80 mm
	8	33	Midland-Odessa Texas	# pattern of fields & oil fields; high- way. Dark patch due to rainstorm. See also AS6-1454	med	137	Vertical	137 mi	0.1 Km	80 mm
	8	45	Cape Kennedy Florida	Launch complex; roads See also V-2-53, VII- 22-26, VII-22-27. Straight coastline South of Cape	low- hazy	(100-175)	Oblique	200 mi	0.3 Km	80 mm
	16	46	Foul Bay Egypt-Red Sea	Straight wadis due to erosion along faults	high	103	Vertical	103 mi	0.1 Km	80 mm
	16	53	Mauritania Sahara Desert	Richat impact crater See also AS9-3050	low light	104	Vertical	104 mi	0.2 Km	80 mm
Gemini V	1	2	Alexandria & Nile Delta	Agriculture; roads & canals See also V-1-4	med	(100-215)	Vertical	125 mi	0.1 Km	80 mm
		4	Libya + Tunisia Mediterranean Coast	Peninsula resembling breakwater. See also V-2-23	med	(100-215)	Oblique	300 mi	0.3 Km	80 mm

<u>Mission</u>	<u>Mag</u>	<u>Frame</u>	<u>Location</u>	<u>Items of Interest</u>	<u>Contrast</u>	<u>Altitude (miles)</u>	<u>Angle of Photograph</u>	<u>Slant Range</u>	<u>Resolution</u>	<u>Focal Length</u>
Gemini V	1	5	Morocco-Atlantic Coast	Signs of Agadir earthquake	high	(100-215)	Vertical	150 mi	0.1 Km	80 mm
		13	Salton Sea & Imperial Valley, California	# pattern of farmland. See also AS9-3287	med	106	Oblique	400 mi	0.3 Km	80 mm
		17	Wilcox Dry Lake Arizona-New Mexico	# pattern of farmland. Roads. See also AS6-1443	high	(100-215)	Vertical	150 mi	0.1 Km	80 mm
		18	El Paso - White Sands Texas-New Mexico-Chihuahua	# pattern of fields in Rio Grande Valley; Roads	high	(100-215)	Vertical	150 mi	0.1 Km	80 mm
		34	Shanghai-Mouth of Yangtze	Roads	low hazy	(100-215)	High Oblique	400 mi	0.4 Km	80 mm
		44	Nile Delta Egypt	Cairo & Ismalia Canal, agriculture. Roads & canals. See also V-1-2	high	(100-215)	Vertical	100 mi	0.1 Km	80 mm
		59	Lake Titicaca Peru-Bolivia	La Paz, Bolivia in picture but not visible	med-dark	(100-215)	Vertical	150 mi	0.2 Km	80 mm
	2	3	Bikini Atoll Marshall Islands	Atoll Reef. See also VII-22-6, X-11-18. Sun glint on ocean	high	130	Vertical	130 mi	0.1 Km	80 mm
		17	Libya-Tripoli	Coastline & fields	high	(100-215)	Vertical	150 mi	0.1 Km	80 mm
		33	Walvis Bay S.W. Africa	Sand dunes & roads See also V-1-4	high	156	Vertical	156 mi	0.1 Km	80 mm
		34	Windhoek S.W. Africa	# pattern of faults	low hazy	156	Vertical	156 mi	0.2 Km	80 mm
		35	Windhoek area S.W. Africa	Linear features, Dunes on faults	low hazy	156	Vertical	156 mi	0.2 Km	80 mm

<u>Mission</u>	<u>Mag</u>	<u>Frame</u>	<u>Location</u>	<u>Items of Interest</u>	<u>Contrast</u>	<u>Altitude (miles)</u>	<u>Angle of Photograph</u>	<u>Slant Range</u>	<u>Resolution</u>	<u>Focal Length</u>
Gemini V	2	53	Cape Kennedy Florida	Roads & launch complex. See also IV-8-45, VII-22-26, VII-22-27	high	127	Vertical	127 mi	0.1	80 mm
		54	Orange River S.W. Africa	Linear features - Faults	med	(100-215)	Vertical	150 mi	0.2 Km	80 mm
	3	27	Guadalupe Island	Cloud eddies. See also V-4-67, X-13-24, X-13-28, XII-8-108	high	(100-215)	Vertical	150 mi	0.1 Km	80 mm
		30	Gulf of California Tiburon Island	Straight sandbars running parallel to coast resemble breakwaters	high	(100-215)	Vertical	150 mi	0.1 Km	80 mm
		50	Iran-Kazir Salt Flats	Circular cone of volcano; roads	med	107	Vertical	107 mi	0.1 Km	80 mm
	4	4	Egypt-Nile Delta	Suez & Ismailia Canals. See also V-1-2, V-4-5	high	(100-215)	Oblique	250 mi	0.3 Km	80 mm
		5	Egypt-Suez Canal Red Sea	Suez Canal: road See also V-4-4	high	(100-215)	Vertical	200 mi	0.2 Km	80 mm
		7	Pensacola-Mobile	Straight coastline; Smoke from 2 forest fires; linear array of clouds	high dark	(100-215)	Vertical	150 mi	0.1 Km	80 mm
		16	Afghanistan- Murghar River	Dust storm	med	(100-215)	High Oblique	500 mi	0.5 Km	80 mm
		45	Iran-Dasht i Lut desert	Scissors fault	low very dark	161	Vertical	161 mi	0.5 Km	80 mm
		50	Cape York Australia	Barrier Reef	med	(100-215)	Oblique	300 mi	0.3 Km	80 mm

<u>Mission</u>	<u>Mag</u>	<u>Frame</u>	<u>Location</u>	<u>Items of Interest</u>	<u>Contrast</u>	<u>Altitude (miles)</u>	<u>Angle of Photograph</u>	<u>Slant Range</u>	<u>Resolution</u>	<u>Focal Length</u>
Gemini V	4	67	Cape Verde Islands	Cloud eddies. See also V-3-27, X-13-24, X-13-28, XII-8-108	high	125	Oblique	250 mi	0.2 Km	80 mm
Gemini VI	B	31	Ras Hafun, Somalia	Straight wadis	high	185	Oblique	200 mi	0.2 Km	80 mm
		35	W. Australia	Lake McLeod	med	185	Oblique	200 mi	0.2 Km	80 mm
		36	W. Australia Shark Bay	Straight coastline	low hazy	185	Oblique	200 mi	0.2 Km	80 mm
		37	W. Australia		low hazy	185	Oblique	200 mi	0.3 Km	80 mm
	C	34	Timbuctu, Niger River	Inundated and dunes, Timbuctu invisible. See also IX-B-50, IX-F-38	low	185	High Oblique	400 mi	0.4 Km	80 mm
Gemini VII	13	19	S.W. Africa-Rocky Point	Coastal road	low dark & hazy	(120-174)	Vertical	150 mi	0.2 Km	80 mm
		37	Haiti	Roads	high	(120-174)	Oblique	250 mi	0.2 Km	80 mm
	17	56	Mexico-Torreon- Comargo	Fault	high	(120-174)	Vertical	140 mi	0.1 Km	80 mm
	17	57	Mexico-Torreon	Fault	high	(120-174)	Vertical	140 mi	0.1 Km	80 mm
	17	58	Mexico-Torreon- Saltillo	Fault	high	(120-174)	Vertical	140 mi	0.1 Km	80 mm
	22	3	Algeria - South of Colomb Bechar	Sand dunes Telephoto	high	139	Vertical	139 mi	0.04 Km	250 mm
		6	Auamotu Archipelago	Atolls See also V-2-3, X-11-18	high dark	(120-174)	Vertical	150 mi	0.2 Km	80 mm

<u>Mission</u>	<u>Mag</u>	<u>Frame</u>	<u>Location</u>	<u>Items of Interest</u>	<u>Contrast</u>	<u>Altitude (Miles)</u>	<u>Angle of Photograph</u>	<u>Slant Range</u>	<u>Resolution</u>	<u>Focal Length</u>
Gemini VII	22	23	Mexico-Gulf Coast	Road along coast	low hazy	(120-174)	Vertical	150 mi	0.2 Km	80 mm
		25	East Coast Florida Titusville-Daytona	Roads; cities; straight coastline	low hazy & dark	(120-174)	Vertical	150 mi	0.2 Km	80 mm
		26	Cape Kennedy Florida	Launch complex; telephoto airfield; straight coastline See also IV-8-45, V-2-53, VII-22-27	low hazy	(120-174)	Vertical	100 mi	0.06 Km	250 mm
		27	Cape Kennedy Florida	Launch complex; roads; straight coastline. Telephoto See also IV-8-45 V-2-53, VII-22-26	med hazy	(120-174)	Vertical	150 mi	0.05 Km	250 mm
		48	Algeria Hoggar Uplift	Swirling rock strata; sand dunes, See also VII-22-49, AS9-3390, AS9-3034	med	(120-174)	Oblique	300 mi	0.3 Km	80 mm
		49	Algeria Plateau Tadameit	Swirling rock strata; sand dunes. See also VII-22-48, AS9-3390, AS9-3034	med	(120-174)	Oblique	200 mi	0.2 Km	80 mm
	24	23	India-Ceylon	Adam's Bridge	med hazy	(120-174)	Vertical	150 mi	0.2 Km	80 mm
		24	India-Ceylon	Adam's Bridge	med hazy	(120-174)	Vertical	150 mi	0.2 Km	80 mm
		25	India-Ceylon	Adam's Bridge	med hazy	(120-174)	Vertical	150 mi	0.2 Km	80 mm
	26	4	Pensacola-Panama City, Florida	Coastline narrow, straight, IR Ektachrome Film	low hazy & dark	148	Vertical	148 mi	0.2 Km	80 mm

<u>Mission</u>	<u>Mag</u>	<u>Frame</u>	<u>Location</u>	<u>Items of Interest</u>	<u>Contrast</u>	<u>Altitude (Miles)</u>	<u>Angle of Photograph</u>	<u>Slant Range</u>	<u>Resolution</u>	<u>Focal Length</u>
Gemini	26	26	Brazil, Ceara Rio Grande de Norte	Clouds IR Ektachrome Film	high	(120-174)	Oblique	200 mi	0.2 Km	80 mm
Gemini IX	B	50	Lake Chad	Inundated Sand Dunes See also VI-C-34, IX-F-38	med	(146-157)	Vertical	150 mi	0.2 Km	80 mm
	C	36	Peru	Straight sections of coastline, Signs of Huascaran Avalanche 1962	med	(146-157)	Vertical	150 mi	0.2 Km	80 mm
		48	Peru-Bolivia	Lake Titicaca, La Paz, Bolivia invisible	med	(146-157)	Oblique	250 mi	0.3 Km	80 mm
		50	Peru-Bolivia	Lake Titicaca La Paz invisible	low dark	(146-157)	Oblique	250 mi	0.3 Km	80 mm
	D	15	Southwestern USA	Contrail and its shadow are visible. See also IX-D-37 XII-11-76, XII-11-147	low dark	(146-157)	High Oblique	400 mi	0.4 Km	38 mm
		37	Los Angeles Area	Contrail . See also IX-D-15, XII-11-76 XII-11-147	high	(146-157)	High Oblique	500 mi	0.4 Km	38 mm
	F	38	Timbuctu Area	Sand Dunes; "Angry Alligator" Agena. See also VI-C-34 IX-B-50	low light	(146-157)	Oblique	250 mi	0.2 Km	80 mm
Gemini X	11	18	Maldiv Islands	Atolls; See also V-2-3, VII-22-6	high	(109-410)	High Oblique	300 mi	0.3 Km	80 mm
		13	Canary Islands	Cloud Vortex; See also V-3-27, V-4-67 X-13-28, XII-18-108	high	(109-410)	High Oblique	400 mi	0.4 Km	80 mm
		28	Gibraltar	Cloud Vortex; See also V-3-27, V-4-67 V-13-24, XII-18-108	med	200	High Oblique	500 mi	0.6 Km	80 mm

<u>Mission</u>	<u>Mag</u>	<u>Frame</u>	<u>Location</u>	<u>Items of Interest</u>	<u>Contrast</u>	<u>Altitude (Miles)</u>	<u>Angle of Photography</u>	<u>Slant Range</u>	<u>Resolution</u>	<u>Focal Length</u>
Gemini X	13	40	Surinam, Paramaribo	Parallel lines of clouds	med	(109-410)	Vertical	200 mi	0.2 Km	80 mm
		44	Mauritania	Levrier Bay	med hazy	(109-410)	High Oblique	400 mi	0.4 Km	80 mm
	14	47	E.Coast Sumatra	Parallel cloud lines	med hazy	(109-410)	Vertical	200 mi	0.3 Km	80 mm
Gemini XI	8	50	N.W. Australia	80 mi beach--coastal road	high	670	Vertical	670 mi	1.5 Km	38 mm
	11	31	Australian desert	80 mi beach -- Admiralty Gulf	med hazy	740	Vertical	740 mi	1.0 Km	80 mm
		34	N.W. Australia	80 mi beach -- Bonaparte Gulf	med hazy	740	Vertical	740 mi	0.8 Km	80 mm
		42	N.W. Australia	80 mi beach -- Port Darwin	low hazy	740	Vertical	740 mi	1.0 Km	80 mm
Gemini XII	8	87	Mauritania	Richat crater	high	(152-177)	Oblique	300 mi	0.7 Km	38 mm
		99	Iran	Zagros Mts.	high dark	(152-177)	Vertical	160 mi	0.3 Km	38 mm
		108	Guadalupe Islands	Cloud vortices; see also V-3-27, V-4-67, X-13-24, X-13-28	med dark	(152-177)	Vertical	160 mi	0.3 Km	80 mm
		147	Egypt-Red Sea	Jet Stream Clouds	med	(152-177)	High Oblique	300 mi	0.4 Km	80 mm
	11	76	S.W. U.S., Baja California	Contrail. See also IX-D-15, IX-D-37, XII-11-147	high	177	High Oblique	400 mi	0.5 Km	80 mm
		126	Cuba	Parallel cloud lines	med dark	(152-177)	Vertical	160 mi	0.2 Km	80 mm

<u>Mission</u>	<u>Mag</u>	<u>Frame</u>	<u>Location</u>	<u>Items of Interest</u>	<u>Contrast</u>	<u>Altitude (Miles)</u>	<u>Angle of Photograph</u>	<u>Slant Range</u>	<u>Resolution</u>	<u>Focal Length</u>
Gemini XII	11	147	Libya-Algeria-Tunisia	Sand dunes; contrail and its shadow. See also IX-D-15, IX-D-37, XII-11-76	med	(152-177)	Vertical	160 mi	0.2 Km	80 mm
	17	17	W. Coast Mexico	Linear cloud features	high	(152-177)	High Oblique	300 mi	0.4 Km	80 mm
		36	Florida-Bahamas	Clouds form an angle: not a contrail	high	(152-177)	Oblique	200 mi	0.3 Km	38 mm
		42	Florida-Bahamas	Clouds form an angle	high	(152-177)	Vertical	160 mi	0.2 Km	38 mm
Apollo 6	2	1435	Baja California, Mouth of Colorado	Sinuuous drainage channel. See also IV-8-3. Possibly 2 boats visible in picture. IR Ektochrome Film	high	138	Vertical	138 mi	0.1 Km	76 mm
		1443	Wilcox dry lake, Ariz-New Mexico, Douglas, Ariz	Smoke plume from factory. See also V-1-17. # pattern of farmland, roads. IR Ektachrome	high dark	135	Vertical	135 mi	0.1 Km	76 mm
		1454	Hobbs-Odessa-Midland, Texas	# farmland; gas & oil fields, roads. IR film. See also IV-8-33	high	131	Vertical	131 mi	0.1 Km	76 mm
		1458	Abilene, Texas	# farmland; Interstate 20, City of Abilene, IR Film	high	129	Vertical	129 mi	0.1 Km	76 mm
		1460	Cisco-Graham Texas	# farmland; Interstate 20; meanders in Brazos River; IR Film	high	128	Vertical	128 mi	0.1 Km	76 mm
		1462	Dallas-Fort Worth Texas	# farmland; Interstate 20; Cities of Dallas & Ft. Worth; IR Film	high	128	Vertical	128 mi	0.1 Km	76 mm

<u>Mission</u>	<u>Mag</u>	<u>Frame</u>	<u>Location</u>	<u>Items of Interest</u>	<u>Contrast</u>	<u>Altitude (Miles)</u>	<u>Angle of Photograph</u>	<u>Slant Range</u>	<u>Resolution</u>	<u>Focal Length</u>
Apollo 9	19	3034	Algeria-Ahaggar Mts.	Swirling rock strata; See also VII-22-48, VII-22-49, AS9 3390	med light	99	Vertical	99 mi	0.1 Km	80 mm
		3050	Mauritania	Richat crater; See also IV-16-53	med light	98	Vertical	98 mi	0.1 Km	80 mm
	20	3128	Cape Hatteras, N. Car.	Sand bars along coastline	high	116	Vertical	116 mi	0.1 Km	80 mm
		3135	Nevada	Lake Mead- Las Vegas	high	129	Vertical	129 mi	0.1 Km	80 mm
	21	3266	Georgia	City of Atlanta; roads	med	113	Vertical	113 mi	0.1 Km	80 mm
		3269	Smoky Mts, Georgia	Road	med	103	Vertical	103 mi	0.1 Km	80 mm
		3273	N. Carolina	Sand bars along coast; smoke from forest fire	med	102	Vertical	102 mi	0.1 Km	80 mm
		3287	Imperial Valley, Calif.	# pattern of fields; roads; See also V-1-13	high	107	Vertical	107 mi	0.1 Km	80 mm
		3290	Phoenix, Arizona	# pattern of fields; roads. City of Phoenix	high	106	Vertical	106 mi	0.1 Km	80 mm
		3299	Dallas-Ft. Worth, Texas	Roads; Interstate 20 Cities of Dallas & Ft. Worth	med	105	Vertical	105 mi	0.1 Km	80 mm
		3300	Red River, La.	Road	med	105	Vertical	105 mi	0.1 Km	80 mm
		3302	Monroe, La.	Road; River meanders See also AS9-3454	high	105	Vertical	105 mi	0.1 Km	80 mm
		3303	Baton Rouge, La.	Meanders & oxbow lakes; Mississippi River	high	105	Vertical	105 mi	0.1 Km	80 mm

<u>Mission</u>	<u>Mag</u>	<u>Frame</u>	<u>Location</u>	<u>Items of Interest</u>	<u>Contrast</u>	<u>Altitude (Miles)</u>	<u>Angle of Photograph</u>	<u>Slant Range</u>	<u>Resolution</u>	<u>Focal Length</u>
Apollo 9	21	3305	Mexicali-Yuma Arizona	Canal	high	105	Vertical	105 mi	0.1 Km	80 mm
		3390	Algeria-Hoggar Mtn. Area	Swirling rock strata. See also VII-22-48, VII-22-49, AS9-3034	med light	90	Vertical	90 mi	0.1 Km	80 mm
		3454	Memphis, Tenn.	River meanders; See also AS9-3302	med	104	Oblique	150 mi	0.2 Km	80 mm
		3463	Houston & Galveston	Roads, # pattern of fields	med	103	Vertical	103 mi	0.1 Km	80 mm
		3566	Birmingham, Ala.	Roads	med	106	Vertical	106 mi	0.1 Km	80 mm

## Bibliography

- M. H. Carr, W. A. Baum, G. A. Briggs, H. Masursky, D. W. Wise, and D. R. Montgomery (1971) Imaging experiment: The Viking Mars Orbiters. *Icarus* 15, .
- S. D. Kilston, R. R. Drummond, and C. Sagan (1966) A search for life on Earth at kilometer resolution. *Icarus* 5, 79.
- H. Masursky, R. Batson, W. Borgeson, M. Carr, J. McCauley, D. Milton, R. Wildey, D. Wilhelms, B. Murray, N. Horowitz, R. Leighton, R. Sharp, W. Thompson, G. Briggs, P. Chandeysson, E. Shipley, C. Sagan, J. Pollack, J. Lederberg, E. Levinthal, W. Hartmann, T. McCord, B. Smith, M. Davies, G. de Vaucouleurs, and C. Leovy (1970) Television experiment for Mariner Mars 1971. *Icarus* 12, 10-45.
- B. C. Murray, M. J. S. Belton, G. E. Danielson, M. E. Davies, G. P. Kuiper, B. T. O'Leary, V. E. Suomi and N. J. Trask (1971) Imaging of Mercury and Venus from a flyby. *Icarus* 15, .
- T. A. Mutch, A. G. Binder, F. O. Huck, E. C. Levinthal, E. C. Morris, C. Sagan, and A. T. Young (1971) Imaging experiment: The Viking Mars Lander. *Icarus* 15, .
- C. Sagan, R. N. Coluelli, S. Q. Duntley, v. R. Eshleman, D. M. Gates, A. Katz, J. Lederberg, H. Masursky, D. G. Rea, W. G. Stroud, V. Suomi, and R. Zirkind (1966). Remote detection of terrestrial life. In "Biology and the Exploration of Mars," C. S. Pittendrigh, W. Vishniac and J. P. T. Pearman, eds. National Academy of Sciences/ National Research Council Publication 1296, Washington, D.C.
- C. Sagan (1970) "Planetary Exploration: The Condon Lectures." University of Oregon Press, Eugene.

## FIGURE CAPTIONS

- Fig. 1. Approximately half the photographs of the Earth are primarily of clouds. Here, turbulent eddies are produced by winds passing over Guadalupe Island, off the coast of Baja California, made visible by the clouds. The tether line which attached the astronaut to the spacecraft during EVA is visible at the right.
- Fig. 2. This photograph shows the coast of North Carolina, including Cape Hatteras and Pamlico Sound. The sandbars off the coast might be mistaken for giant engineering works by a visitor from space, but are entirely natural. At the right are clouds of smoke, possibly from a forest fire. They are easily distinguished from the water clouds at the top.
- Fig. 3. A clear example of intelligent life on Earth. A rectangular grid of irrigated fields in the Western United States is strikingly illustrated in this photograph of the Imperial Valley, Mexicali, and part of the Salton Sea.
- Fig. 4. This photograph shows the area surrounding Midland and Odessa, Texas. The dark area to the upper left was caused by a rainstorm in the area a few hours before this photo was taken. The rectangular grid pattern of fields and roads serving oil wells in the area is apparent over most of the area. A new highway between Midland and Odessa can be seen near the center.
- Fig. 5. This photograph shows the cities of Dallas and Fort Worth, Texas. Large urban areas such as these, and the

straight lines of roads are among the major signs of intelligent life on Earth detectable at 0.1 km resolution.

Fig. 6. This photograph was taken on infrared Ektachrome film for purposes of haze penetration and studies of vegetation, which is bright in reflected near infrared light and gives the photo a reddish color. It covers portions of Arizona and New Mexico. The white area near the center is Wilcos Dry Lake, and is surrounded by the grid pattern of irrigated fields. At the left is another example of "intelligent" life on Earth -- atmospheric pollution in the form of a plume of smoke from a factory in Douglas, Arizona.

Fig. 7. Cairo is the patch of slightly greyer brown at the base of the Nile Delta. The fine lines interlacing the Delta are roads and irrigation canals. These kinds of roads in the Nile Delta antedate the Industrial Revolution. The pattern here, and the grid pattern of the Western United States are both clearly indicative of intelligent life. To the left, the Ismalia Canal cuts through the desert, connecting Cairo with the Suez Canal. Right and left have inadvertently been reversed in the printing of this photo of Cairo and the Nile Delta.

Fig. 8. Gemini V -4-67. Regularities in cloud geometries near the Cape Verde Islands.

Fig. 9. Gemini XII -11-126. Parallel linear arrays of clouds over Cuba. Again, regular geometry does not necessarily imply biology.

- Fig. 10. Gemini XII - 17-42. Two lines of clouds intersect over the Bahamas to form an oblique angle to the left of center. Close inspection shows that they are not contrails since they show the patchy structure of the other clouds in the area.
- Fig. 11. Gemini XII -8-147. Jet stream clouds over Egypt and the Sudan do not closely resemble contrails.
- Fig. 12. Gemini IX - D-15. A jet aircraft contrail and its shadow are visible in this photograph of the Southwestern United States. An extraterrestrial observer would probably consider such contrails as evidence of a terrestrial technological civilization.
- Fig. 13. Gemini IX -D-37. Another contrail is visible in this photograph of the Los Angeles area. Los Angeles is hidden by smog.
- Fig. 14. Gemini IV -6-9. In the lower part of this photograph the Hsiang River in Hunan Province, China, contains several linear sections, giving rise to an unusual geometric pattern. An extraterrestrial observer might suspect that these represent large scale engineering projects.
- Fig. 15. AS9-3303. This photograph shows the meanders and oxbow lakes left by the Mississippi River near Memphis, Tennessee.
- Fig. 16. AS6-2-1435. This photograph of the mouth of the Colorado River contains two peculiar features. The first is the bright corkscrew in the upper center. It is apparently a tidal drainage channel outlined by salt flats. The

second is the two bright dots at the lower right, which may possibly be boats.

Fig. 17. Gemini V -2-33. A field of sand dunes occupies the lower portion of this photograph of the Walvis Bay area, S. W. Africa. The regular linear pattern, however, could probably be interpreted by an extraterrestrial visitor as a natural phenomenon. The sandbar blocking the bay at left, however, might be interpreted as a breakwater or dam or other large engineering work. Roads are marginally visible in the area not covered by the dunes.

Fig. 18. Gemini V -3-30. Two instances of sandbars forming straight lines parallel to the coast are shown in this photograph of Tiburon Island in the Gulf of California. These might be interpreted as artificial harbors, but they are not.

Fig. 19. Gemini VI -C-34. The dark striations in this photograph are sand dunes inundated by the Niger River. Timbuctu is in the photograph, further to the right near the Niger River, but is invisible due to its low contrast.

Fig. 20. Gemini VII -22-3. This is a telephoto image of seif dunes in Southern Algeria. Their semi-regular nature is readily apparent.

Fig. 21. Gemini VII - 22-49. The geometry in this image is due to a field of sand dunes near the center and the peculiar swirling rock strata below. The region is extremely inaccessible, south of the Hoggan Mountains in Algeria. Natural gas has been found in the area of the peculiar rock strata.

- Fig. 22. AS9-3050. The spectacular Richat formation in Mauritania is visible in the lower right. It is apparently a fossil meteorite crater, since coesite, a high pressure modification of quartz, has been found there.
- Fig. 23. Gemini V -3-50. Two volcanic cones are visible near the bottom of this photograph of the Kazir salt flats in Iran. Roads are also faintly visible.
- Fig. 24. Gemini V -4-5. This photograph shows the Suez and Ismailia Canals in the Egyptian desert. The Ismailia Canal at the top center appears much broader and darker than the Suez Canal because of the vegetation.
- Fig. 25. Gemini VII -22-6. This is a photograph of six atolls in the Auomotu Archipelago. It seems very unlikely that the biological origin of those islands would be deduced even by a very intelligent extraterrestrial observer, in the absence of prior knowledge of life on Earth.
- Fig. 26. Gemini V -1-13. This photograph shows the Imperial Valley and Salton Sea in Southern California. The grid pattern of irrigated fields is visible very close to the resolution limit.
- Fig. 27. Gemini V -1-18. The Rio Grande Valley near El Paso, Texas is shown here. The grid pattern of farmland is much more apparent than in the preceding photograph. This pattern is characteristic of the Western United States. A different pattern is visible e.g., in Fig. 7 of the Nile Delta. To an extraterrestrial observer, however, both patterns would be indicative of intelligent life.

Fig. 28. Gemini V -2-53. The launch complex at Cape Kennedy, Florida from which the photographers of the preceding 27 figures were launched, is shown here, with other roads and bridges in the area plainly visible. The beach to the south of the Cape superficially resembles the roads, but closer inspection reveals that the beach is much wider than the roads, and is not so straight.

Fig. 29. Photographic detectivity of planetary biology. Threshold for detection of contemporary life on Earth, determined from this and other studies, is shown by the rippled pattern. This and two other possible detectivity thresholds are compared with present and future coverage of Mars. At the present time a civilization of contemporary terrestrial advancement and extent on Mars would not have been discovered.



NOT REPRODUCIBLE

Figure 1.

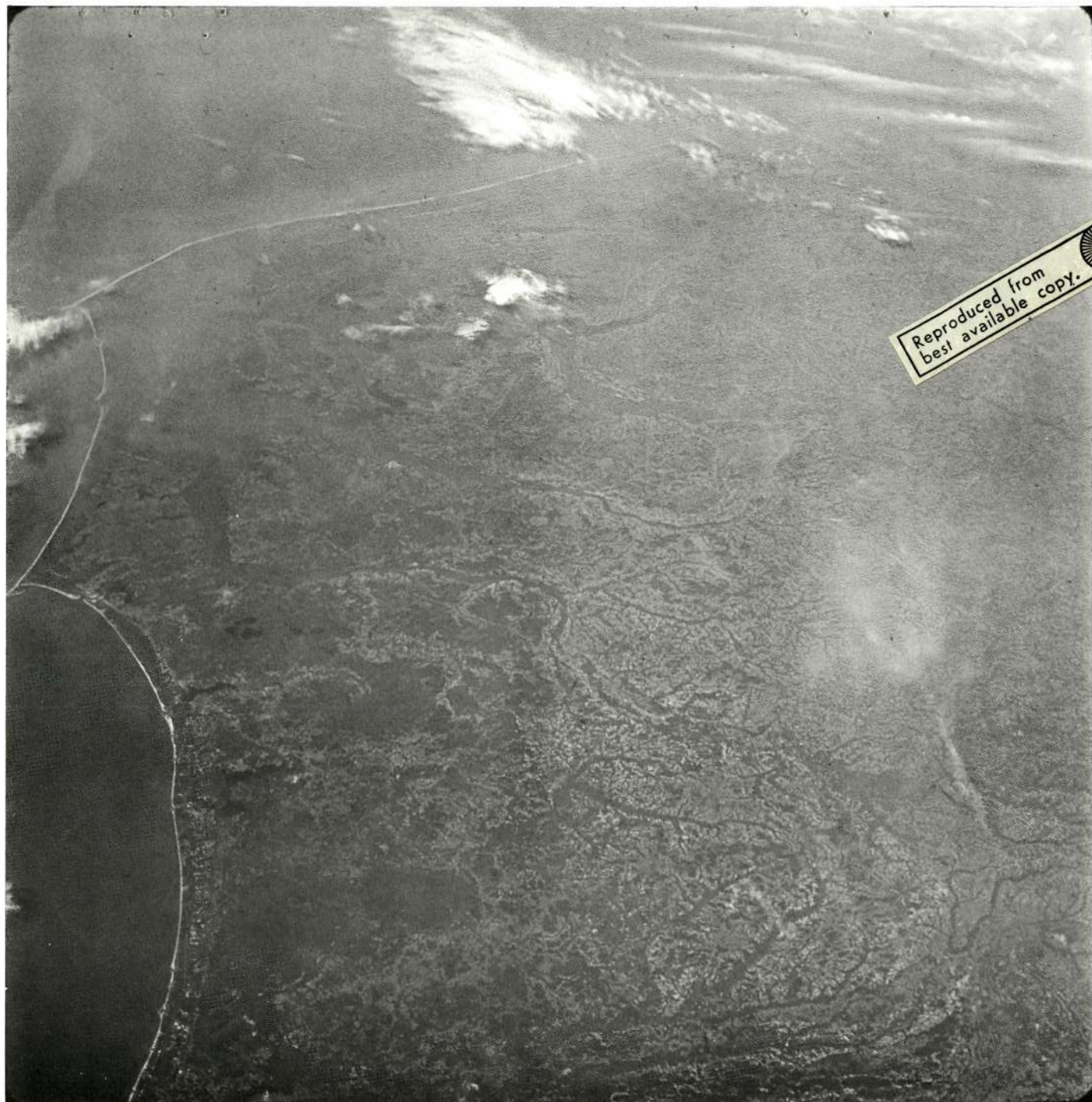


Figure 2.

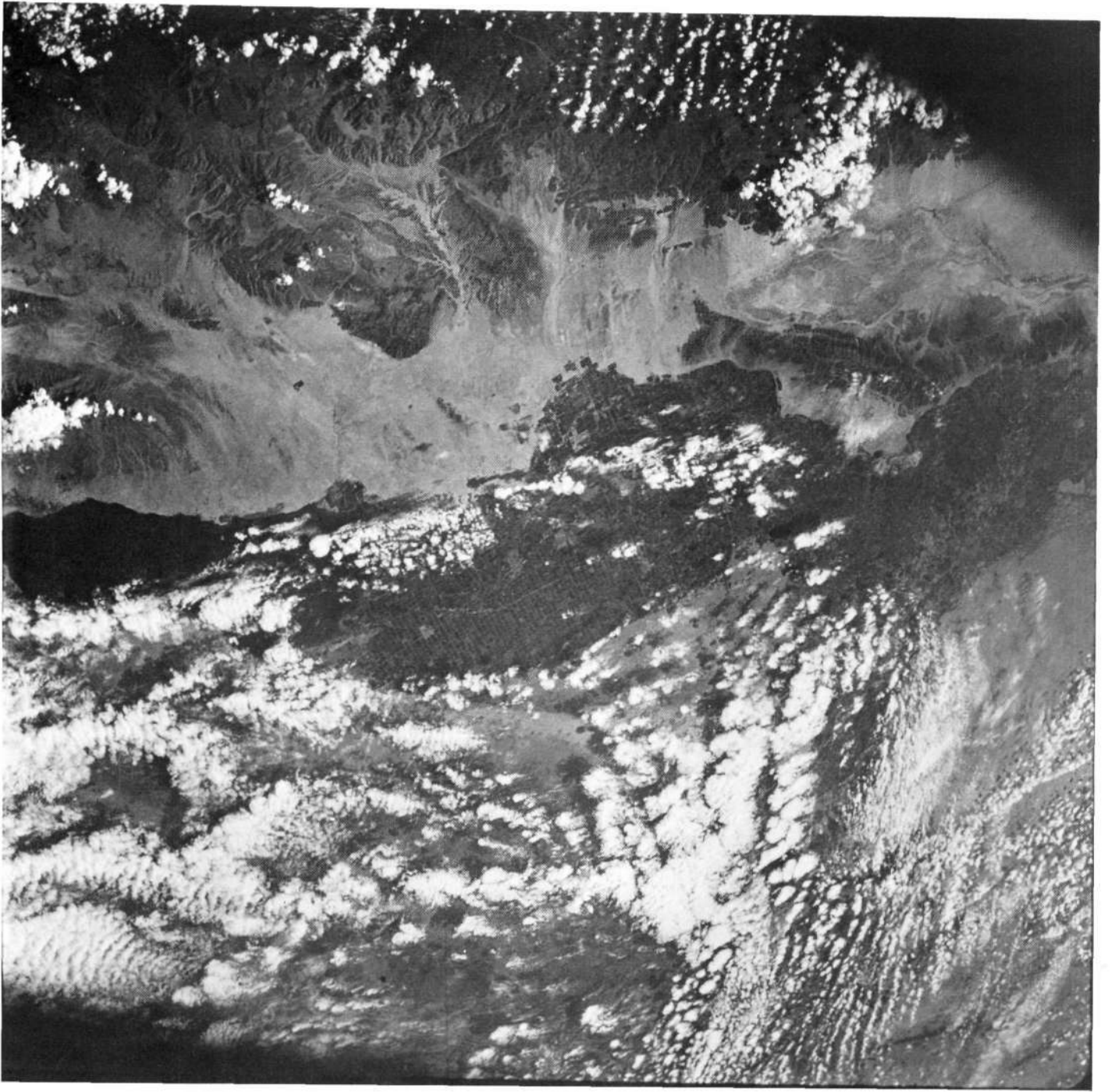


Figure 3.

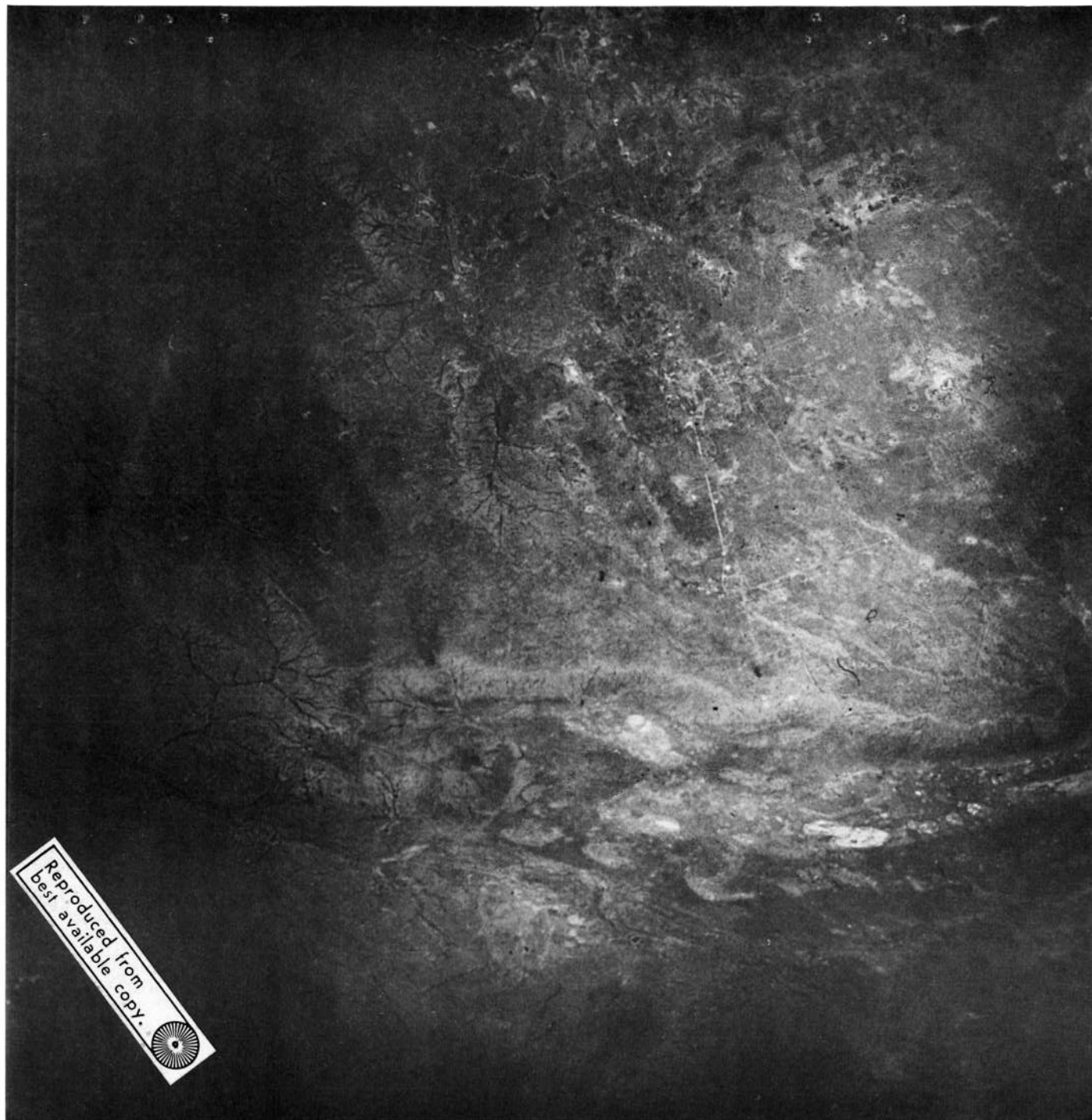


Figure 4.

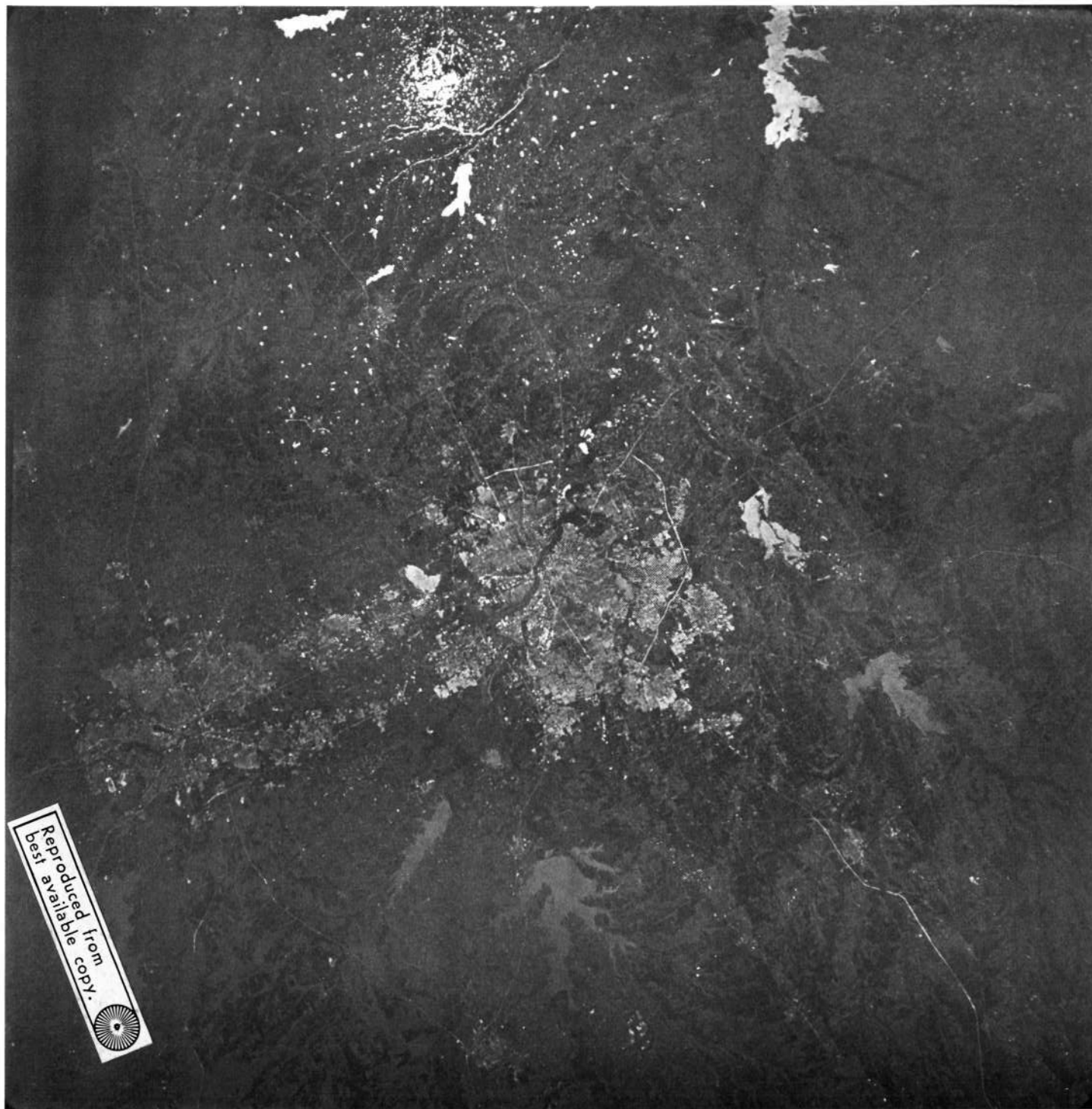


Figure 5.



Figure 6.



Figure 7.

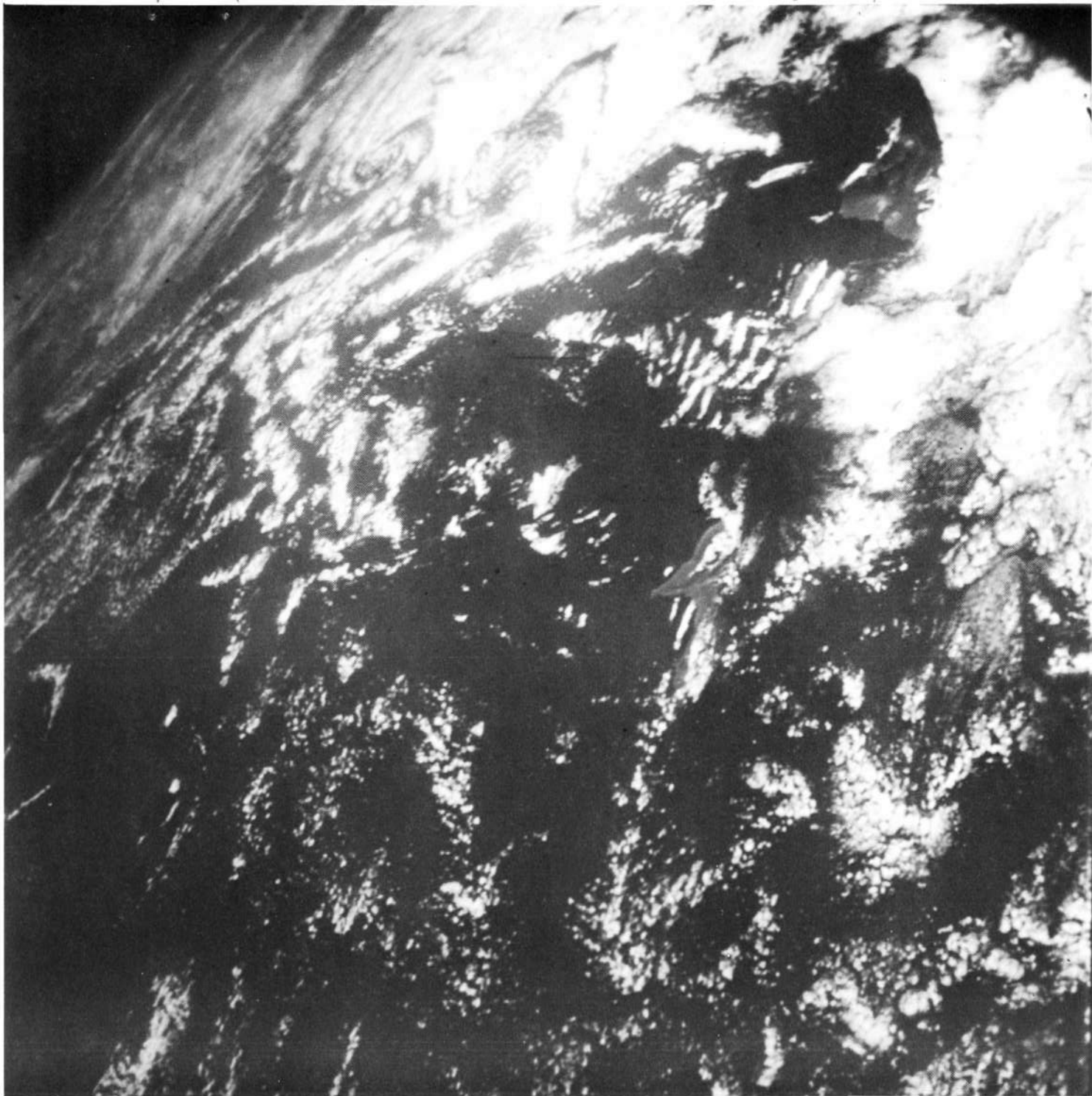


Figure 8.

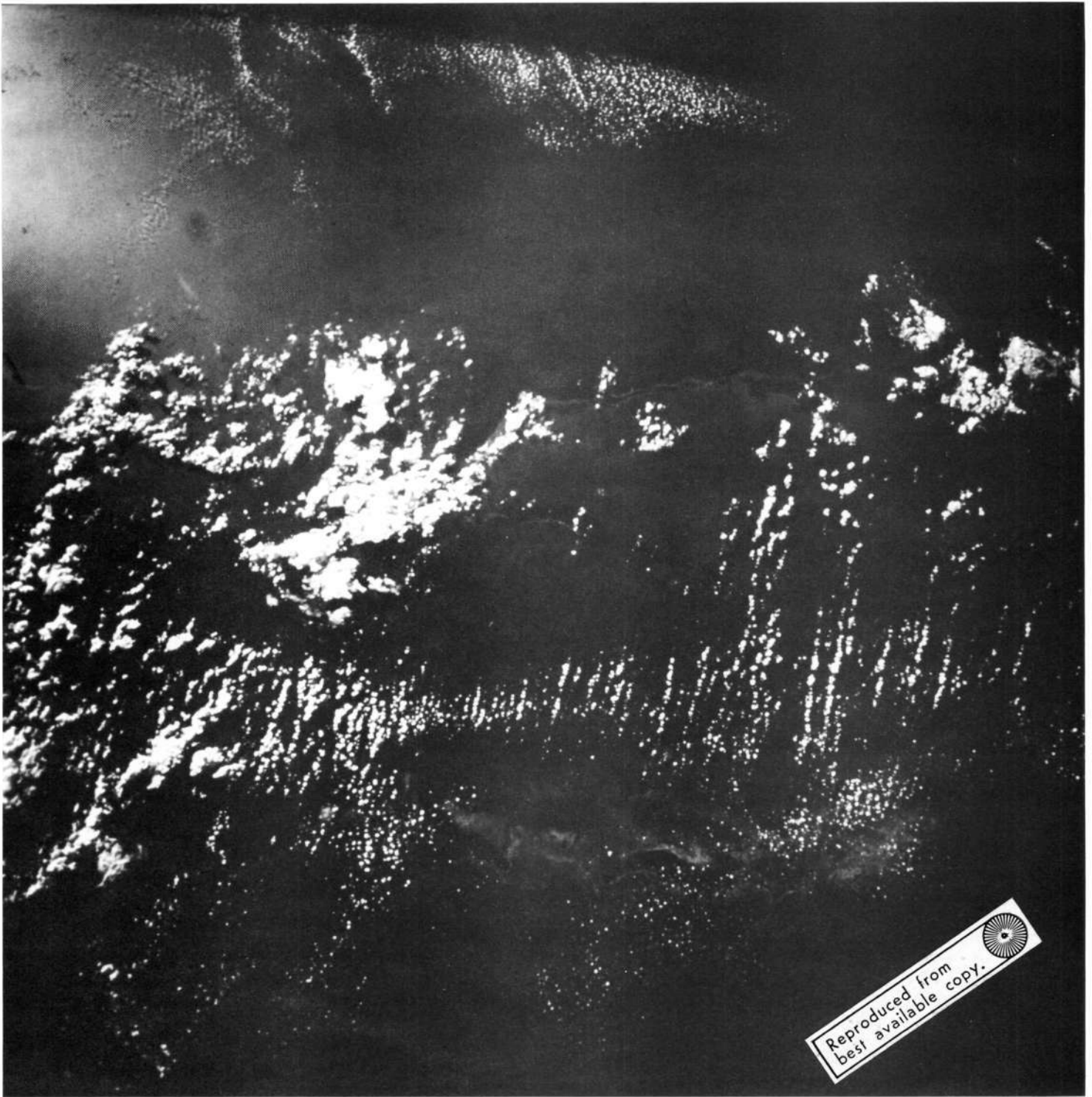


Figure 9.



Figure 10.

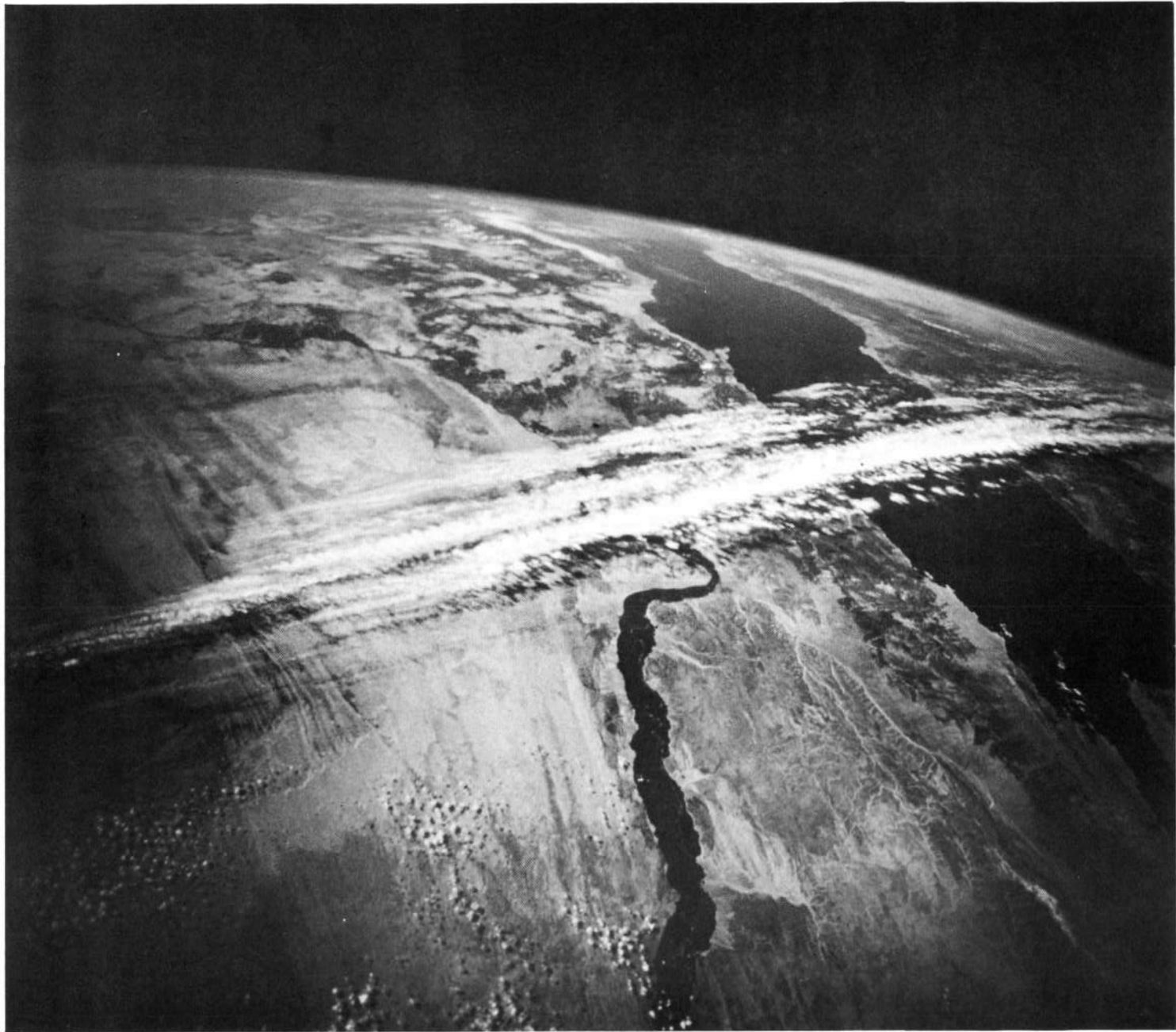


Figure 11.



Figure 12.



Figure 13.

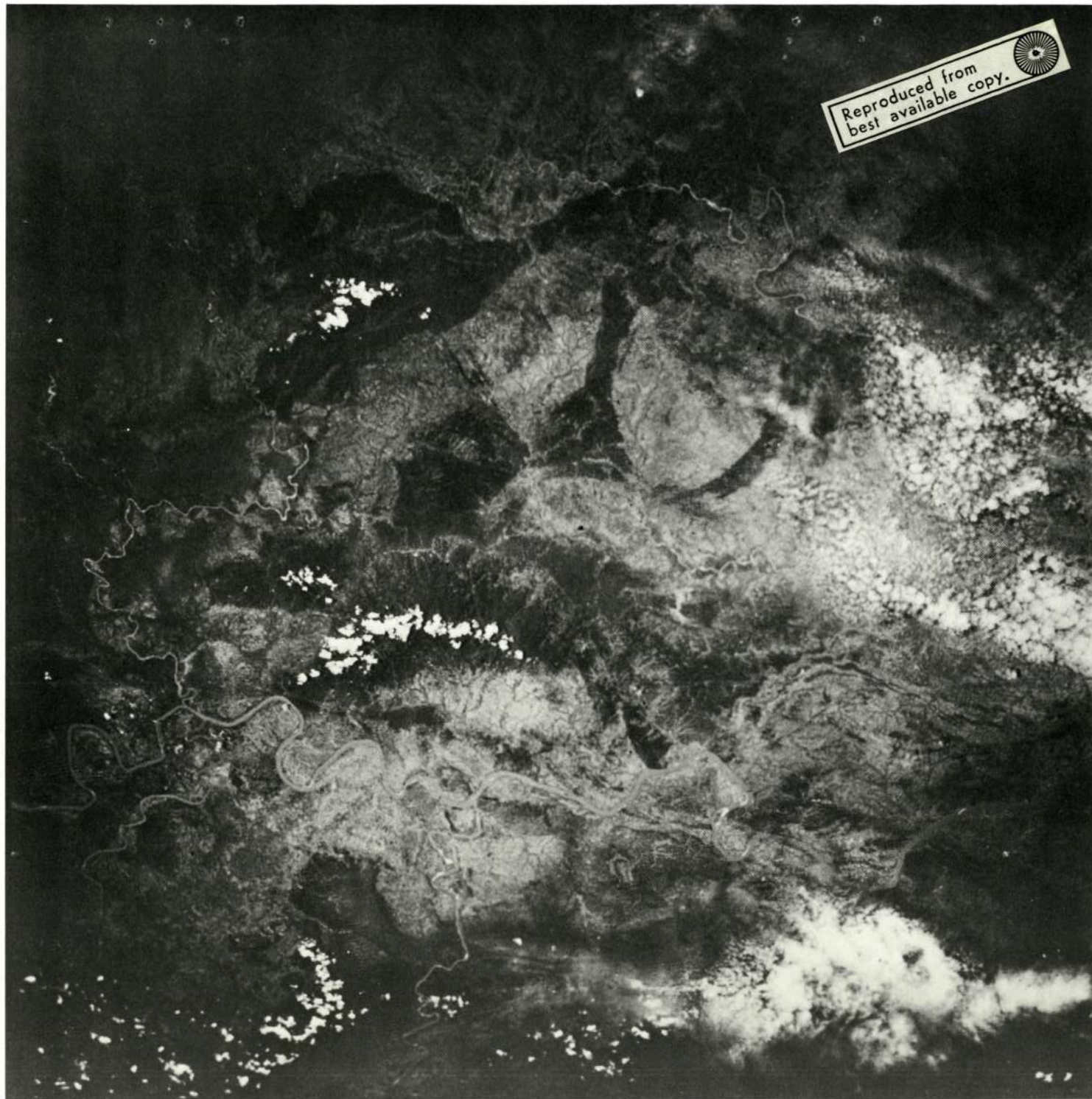


Figure 14.

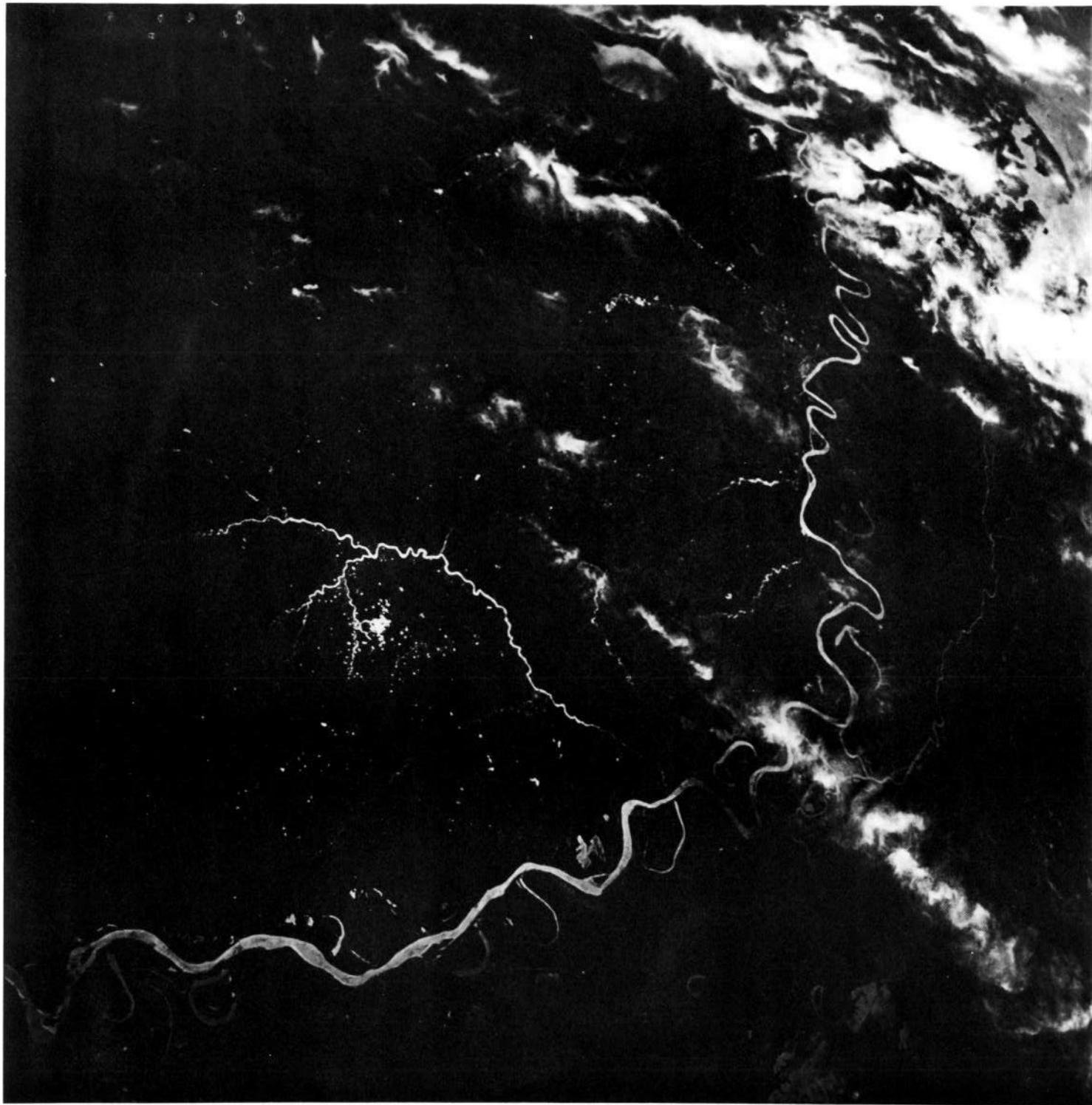


Figure 15.

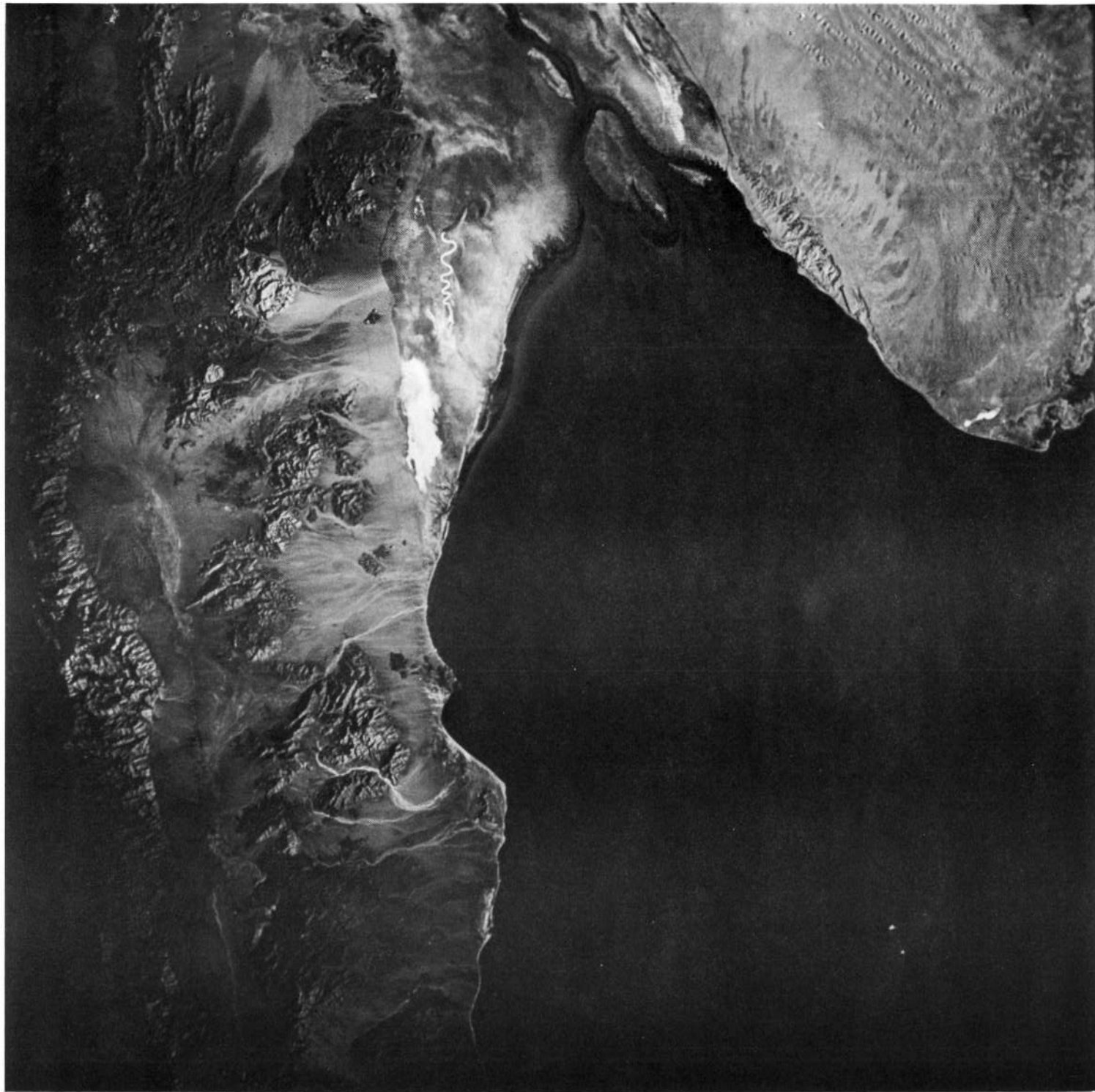


Figure 16.



Figure 17.

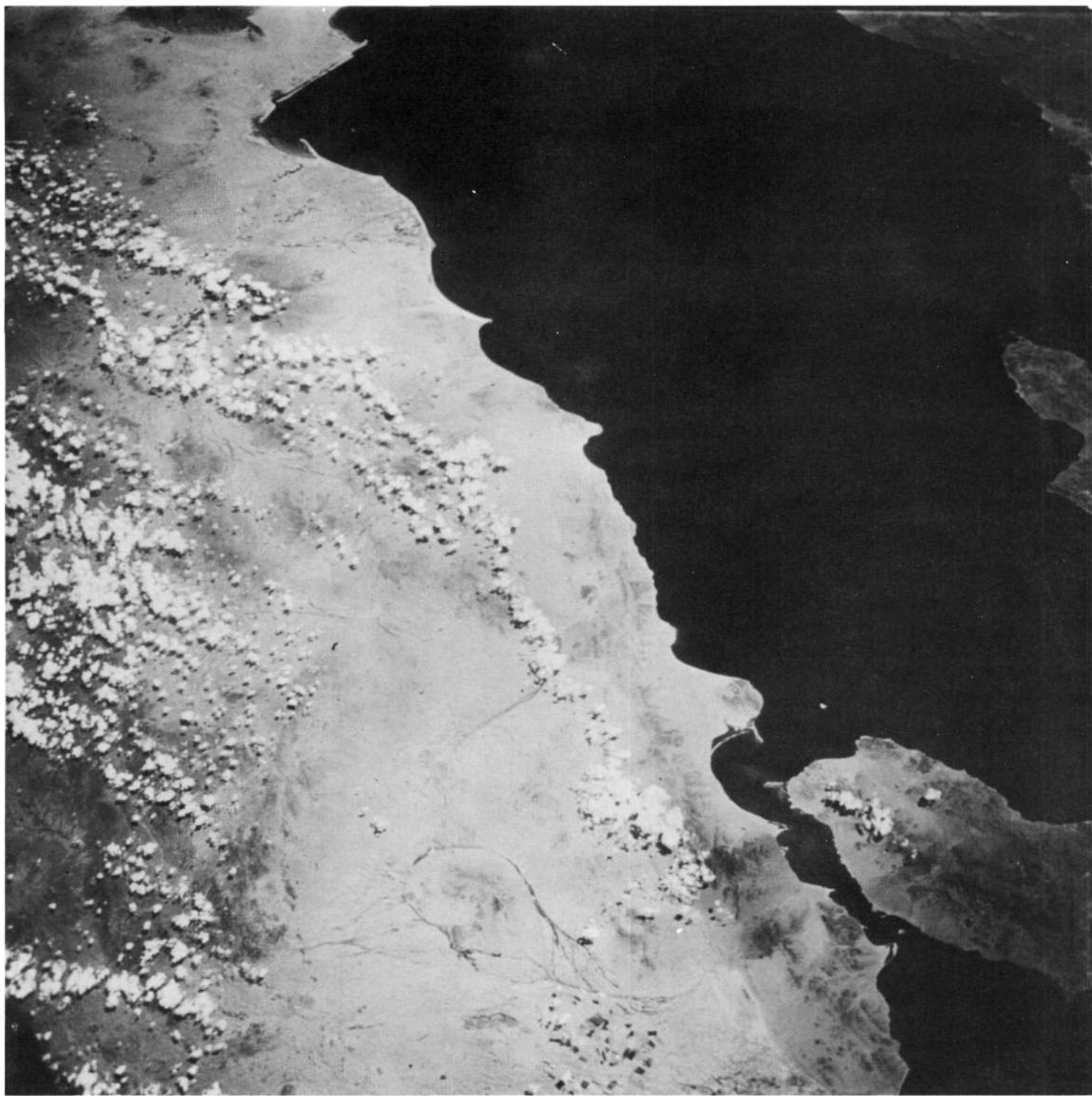


Figure 18.



Figure 19.

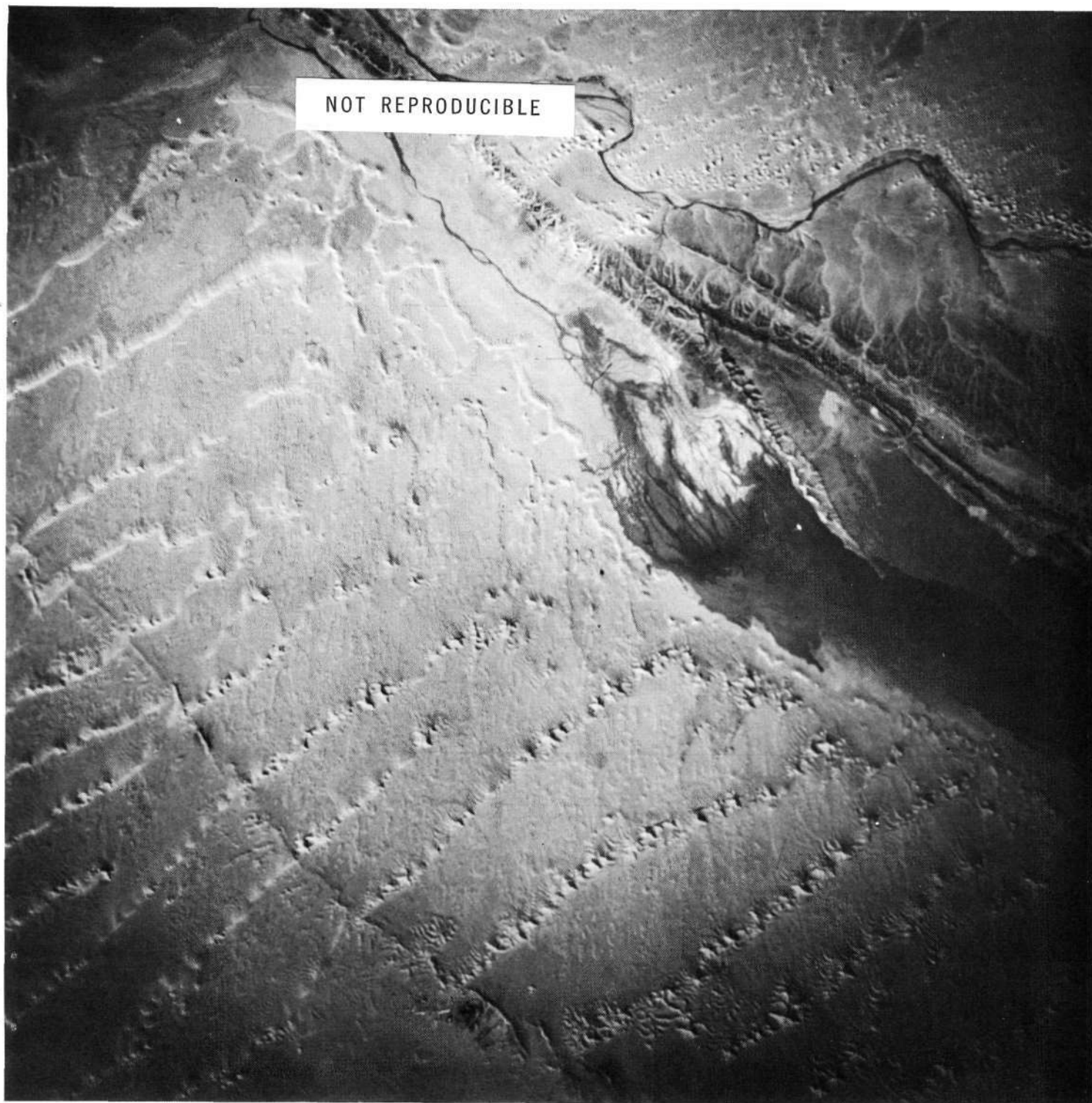


Figure 20.



Figure 21.



Figure 22.



Figure 23.



Figure 24.

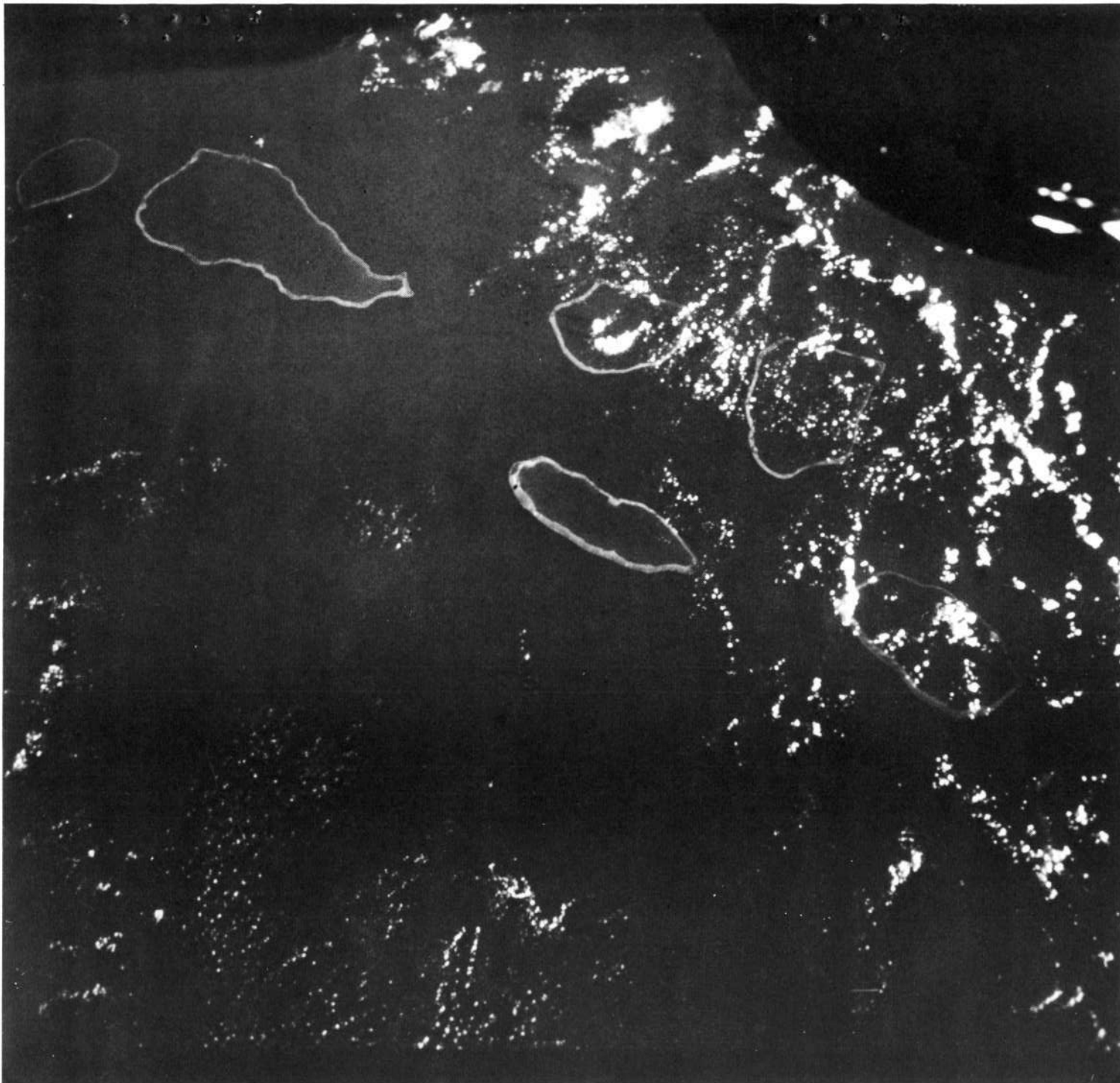


Figure 25.



Figure 26.

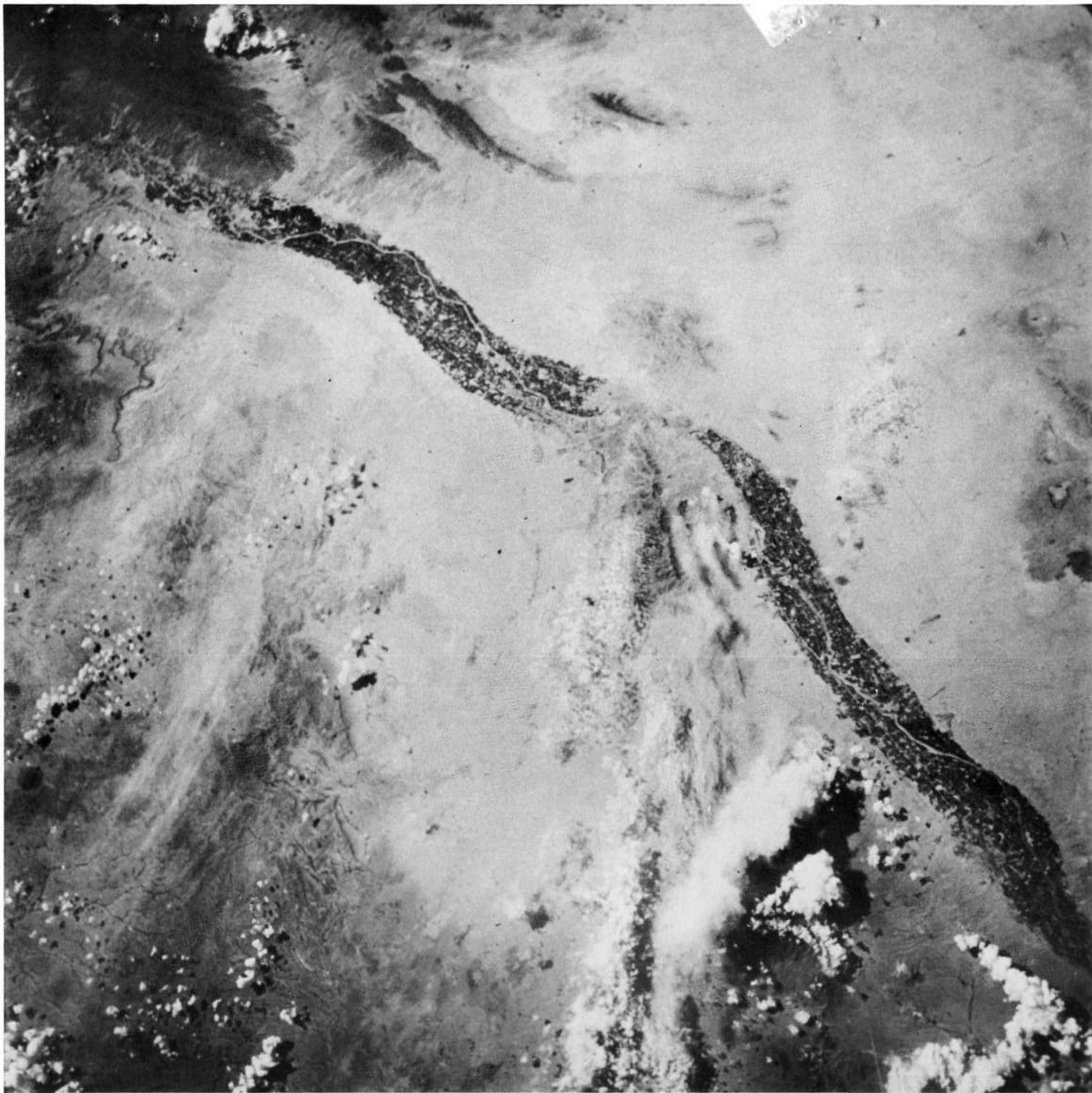


Figure 27.

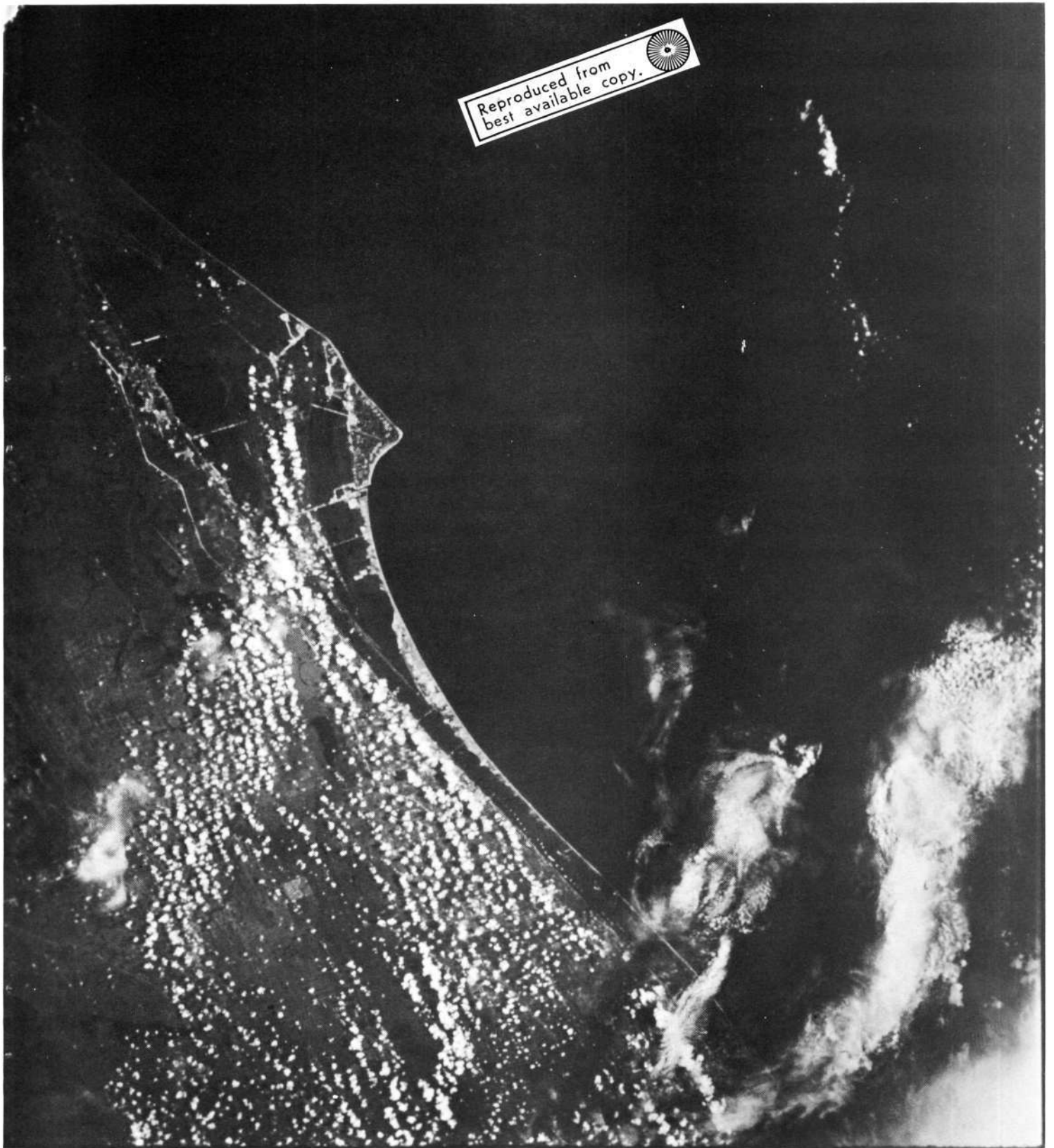


Figure 28.

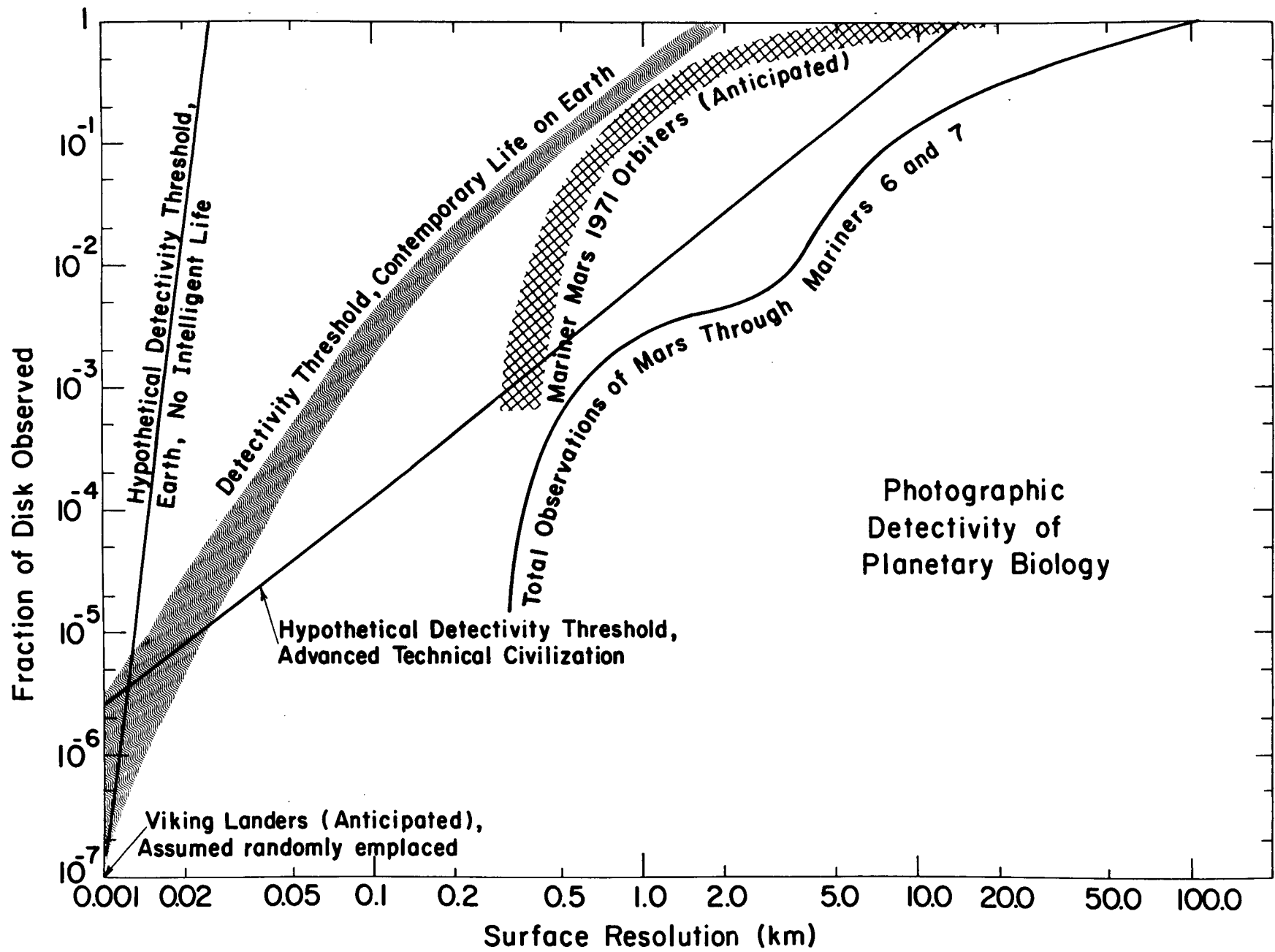


Figure 29.